Gold Bull (2013) 46:257–265
DOI 10.1007/s13404-013-0115-8

ORIGINAL PAPER

In vivo uptake and cellular distribution of gold nanoshells in a preclinical model of xenografted human renal cancer

Mariana Pannerec-Varna · Philippe Ratajczak · Guilhem Bousquet · Irmine Ferreira · Christophe Leboeuf · Raphaël Boisgard · Guillaume Gapihan · Jérôme Verine · Bruno Palpant · Emmanuel Bossy · Eric Doris · Joel Poupon · Emmanuel Fort · Anne Janin

Published online: 17 November 2013

Abstract Large-sized gold nanoparticles, promising imaging and therapeutic tools in human cancer, need long-term studies evaluating tissue bio-distribution in blood, organs and tumor. In a preclinical model of mouse xenografted with human renal cancer, we analysed the bio-distribution of a single dose (160 μg/kg) intravenously injected of poly-ethylene glycol (PEG)ylated gold nanoshells (~150 nm), in blood, normal and tumoral tissues. Using inductively coupled plasma mass spectrometry (ICP-MS), dark field and electron microscopy, we performed a sequential study of nanoshell uptake and distribution in the tumor. We also studied microscopically the organs most sensitive to efficient anticancer drugs to detect a possible long-term toxicity. Gold quantities significantly decreased in blood between early and late time points, whereas they significantly increased in liver and spleen. In addition, gold nanoshells did not induce any tissue damage, such as necrosis, inflammatory infiltrate or fibrosis in mouse liver, spleen, kidney or bone marrow after 6 months. In human renal cancer xenografts, ICP-MS showed an early decrease of gold, with 1-week stability before decrease at Day 15. Dark field microscopy showed gold particles within the vessel lumen 5 to 30 min after nanoshell injection, while 24 h later, gold particle distribution was mainly intracellular. Electron microscopy identified nanoshells within blood vessels at 5 and 30 min, within endothelial cells at 3 and 6 h and within cytoplasms of macrophages in the tumoral tissue after 24 h. In conclusion, no toxicity was observed in mice 6 months after administration of PEGylated gold nanoshells and the distribution kinetics progressed from intravascular flow at 30 min to intratumoral cells 24 h later.

Electronic supplementary material The online version of this article (doi:10.1007/s13404-013-0115-8) contains supplementary material, which is available to authorized users.

M. Pannerec-Varna (✉) · P. Ratajczak · G. Bousquet · I. Ferreira · C. Leboeuf · G. Gapihan · J. Verine · A. Janin (✉)
Université Paris Diderot, Sorbonne Paris Cité, UMR-S 728, 75010 Paris, France
e-mail: mariannavarna@yahoo.fr
e-mail: anne.janin728@gmail.com

M. Pannerec-Varna · P. Ratajczak · G. Bousquet · I. Ferreira · C. Leboeuf · G. Gapihan · J. Verine · A. Janin
INSERM, U728, 75010 Paris, France

R. Boisgard
Commissariat d'Energie Atomique et aux Energies Alternatives, SHFJ, INSERM, U1023, 91401 Orsay, France

B. Palpant
Laboratoire de Photonique Quantique et Moléculaire, Ecole Centrale Paris, Grande Voie des Vignes, 92295 Châtenay-Malabry Cedex, France

E. Bossy · E. Fort
Institut Langevin, ESPCI ParisTech, 75238 Paris, France

E. Doris
Service de Chimie Bioorganique et de Marquage, CEA, iBiTecS, 91191 Gif-sur-Yvette, France

J. Poupon
Laboratoire de Toxicologie biologique, AP-HP-Hôpital Lariboisière, Paris 75010, France

J. Verine · A. Janin
Laboratoire de Pathologie, AP-HP-Hôpital Saint-Louis, Paris 75010, France

Keywords Gold nanoshells · Mouse xenograft · Human renal cancer · Sequential study · Tissue biodistribution · Long-term tolerance

Introduction

Gold nanoparticles are now synthesised into a large variety of forms. Only some of them are suitable for in vivo hyperthermia. A recent comparative study of small-sized gold nanoparticles including nanorods, nanocages and nanohexapods demonstrated the value of nanohexapods for in vivo photothermal destruction using ^{18}F-fluorodesoxyglucose positron emission tomography/computed tomography [1]. Large-sized gold nanoparticles (NPs) such as nanoshells about 150 nm in diameter are also promising tools for imaging and therapeutic approaches in cancer [2].

In preclinical models, the spherical particles of silica–gold nanoshells have shown optical properties for imaging and photothermal targeted therapy [3, 4]. In addition, a polyethylene glycol (PEG) coating reduces the adsorption of blood serum proteins to the nanoparticles [1]. Liu et al. [5] also demonstrated that PEGylation is a key factor that governs the fate of gold nanoparticles in the animal organisms and their accumulation in target organs. PEGylated gold nanoshells enter more easily into organs and tissues [6]. Encouraging results showed, at the early checkpoint of 7 days after injection, the absence of toxicity of PEGylated small-sized gold nanoparticle in liver spleen, kidney, heart and lung [1].

In the field of cancer, the possibility to link antibodies to nanoshells using PEG enables the use of these biocompatible nanoshells for the delivery of drugs to targeted tumor cells. The goal of such innovative treatment is double to enhance the drug effect on targeted tumor cells and to reduce the toxic effect of the anticancer drug on normal organs. A prerequisite for the use of these biocompatible nanoparticles in oncology daily practice is to check in vivo their tolerance in the long-term and on the organs that are the most sensitive to efficient anticancer drugs, particularly the liver, bone marrow, kidney, heart and lung [7, 8].

To perform this study, we used human tumor xenografts in immunodeficient mice. This in vivo model enables sequential analyses in the different physiological compartments represented by blood, normal and tumoral tissues [9], [10]. In this preclinical model, we studied human renal cancer, since this highly vascularised cancer frequently develops haematogenous metastases and resists to anticancer drugs at non-toxic therapeutic doses [11]. We performed a sequential analysis of uptake and distribution of large-sized PEGylated gold nanoshells and focussed the study on their intracellular distribution in the xenografted human cancers, as well as on their long-term tolerance in normal mouse organs.

Experimental section

Nanoparticle characteristics

Gold nanoshells composed of a ~20-nm Au shell around a ~130-nm silica core and PEGylated (MW=5,000) were purchased from Nanospectra Biosciences (Houston, TX, USA). The nanoparticles were characterised using transmission electron microscopy (TEM) and the absorbance spectrum was evaluated with a Genesys 10S UV-VIS spectrophotometer (Thermo Scientifique, France).

Dynamic light scattering (DLS) and zeta potential measurements were carried out with a Nanosizer ZS90 instrument (MALVERN) at 25 °C. Hydrodynamic diameters were obtained using the cumulant method.

PEG density is estimated at ~10–15 pmol/cm^2 (about 13,000 molecules/particle) (Nanospectra Biosciences, TX, USA).

Human renal cancers and mice

For the xenografts, human renal cancer cell carcinoma samples were taken from surgical pieces for Tumorothèque of Hopital Saint Louis by pathologists, after the tumoral tissue necessary to establish the diagnostic had been taken. Informed consent for the use of the tumor sample for research was obtained for each patient. The study was approved by the University Board Ethics Committee and conducted in accordance with the Declaration of Helsinki.

The animal study was approved by the Ethics Committee for animal experimental studies of the University Institute board. NMRI/nude 7-week-old female mice purchased from Janvier (R. Janvier, France) were maintained in specific pathogen-free animal housing.

Ten cubic millimeters of human renal cancer were grafted subcutaneously on mice, under xylasin (10 mg/kg body weight) and ketamin (100 mg/kg body weight) anaesthesia. The follow-up was performed daily and included a clinical score and assessment of tumor growth. Xenografted tumors were measured in two perpendicular diameters with a calliper every day and calculated as $V = L \times l^2/2$, L being the largest diameter (length), l the smallest (width) [12]. Daily, mice were weighed and assessed for behavioural changes and all data were recorded using the FileMakerPro software.

Pharmacokinetics in mice

At different time points and on different organs, we quantified the amount of gold and also assessed a possible toxicity in nude mice and in mice xenografted with human renal cancer.

Gold nanoshells administration

In normal nude mice, gold nanoshells were intravenously injected with 100 μL NPs (3×10^9 NP/mL) ($n=5$) or with PBS as control ($n=3$). In nude mice, xenografted with human renal cancer gold nanoshells were intravenously injected with 100 μL NPs (3×10^9 NP/mL) ($n=5$) or with PBS as controls ($n=3$). After injection, mice were weighed and assessed daily for behavioural changes and all data were registered using the FileMakerPro software.

Sequential blood and tissue sampling

For all mice, the whole blood, heart, kidney, lung, liver, spleen, ovary, adrenal gland, lymph node and brain were systematically sampled. For xenografted mice, a sample from the tumor was also taken. The time points for sampling for normal nude mice were 1, 7 and 15 days and 1, 2, 3 and 6 months. The time points for sampling for xenografted nude mice were 5 and 30 min, 2 and 6 h and 1, 7 and 15 days to respect the ethic rules regarding maximal tumor growth. All tissue samples were cut into three parts: one part was snap-frozen for inductively coupled plasma mass spectrometry (ICP-MS) analysis, another part was glutaraldehyde-fixed for electron microscopy and a third was formalin-fixed and paraffin-embedded for dark field microscopy analysis and histological analysis.

Spectrometric analyses in blood and tissue samples

To quantify the gold content in blood and tissue samples at the different time points described above, ICP-MS was performed. Fresh samples were weighed. After drying at 80 °C overnight, they were weighed again and digested in nitric acid/HCl (Sigma). Remaining minerals were analysed using ICP-MS (Elan DRCe, Perkin Elmer, Les Ulis, France). Samples were nebulized in an argon plasma (6000–8000 °C). The ions formed by nebulization were extracted from the plasma, introduced into a mass spectrometer and separated according to their mass on charge ratio (m/z). Gold content was measured at mass 197, a level at which no interference occurs. The detection limit was 1 ng/L.

Gold nanoshell distribution and assessment of toxicity in the different mouse organs

In the different tissue samples systematically taken during autopsies of mice performed at different time points from 1 day to 6 months, histological analyses were performed on hematoxilin eosin staining to assess whether tissue damages linked to toxicity could be detected. In the organs from mice euthanised early (between 1 and 15 days), particular attention was paid to the following features: acute hepatotoxicity with hepatocyte necrosis and inflammatory infiltrate in the portal areas; hypoplasia or complete aplasia of the bone marrow; acute nephrotoxicity with endothelial damage, fibrin deposit in the glomerular areas and necrosis of epithelial tubular cells; cardiotoxicity with endocardial damage. In the organs from mice euthanised at late time points (1, 2, 3 and 6 months), particular attention was paid to the following features of long-term toxicity: fibrosis and inflammatory infiltrate in the liver; glomerular sclerosis and interstitial fibrosis with inflammatory infiltrate in the kidney; diffuse interstitial fibrosis and inflammatory infiltrate in the lung; and possible bone marrow fibrosis or brain damage.

Assessement of gold nanoshell distribution in xenografted human renal cancer

The distribution of gold nanoshells in xenografted human renal cancer was assessed using dark field microscopy and TEM to analyse the different types of cells within the tumor.

Dark- field microscopy

Five-micromillimeter-thick tissue sections from xenografted human renal cancer were studied using a microscope (Olympus AX, Tokyo, Japan) equipped for both bright field and dark field microscopy. Using bright field, we could focus our analyses on tumoral cells and avoid areas of necrosis. Using dark field on the tumor area identified with bright field microscopy, we could assess the distribution and the relative density of the nanoparticles. Images were captured at ×40 magnification, on the same tumor areas successively analysed using bright field and dark field microscopy.

Transmission electron microscopy

After fixation in 2 % glutaraldehyde in caccodylate buffer, the samples of human renal cancers were embedded in Epon resin. Ultrathin sections were observed using a Hitachi HF-2000 transmission electron microscope (Hitachi, Tokyo, Japan). TEM analyses focussed on the presence of gold nanoshells in the different types of cells observed in the human renal cell cancer: tumoral epithelial cells, vascular endothelial, smooth muscle and pericyte cells, cells from the inflammatory infiltrate including macrophages, and fibroblasts and fibrocytes from the conjunctive stroma.

Statistics

All data were expressed as mean results ± SEM (standard error of mean). The paired Student's t test was used for statistical analysis. A p value of less than 0.05 was taken to indicate statistical significance.

Results and discussion

We studied here in vivo uptake and cellular distribution of gold nanoshells in a preclinical model of xenografted human renal cancer.

For this study, we chose gold-silica nanoshells with a size between 130 and 150 nm because (i) these large nanoshells are suitable for imaging and hyperthermia in vivo [13] and (ii) gold is well tolerated and does not induce toxicity in human beings after intravenous or intra-articular injection [14].

We studied gold–silica nanoshells coated with PEG because PEG polymers form a hydrophilic layer and sterically block the electrostatic or hydrophobic interactions with opsonins [15]. These plasma proteins are less adsorbed on nanoshell surfaces, reducing their aggregation and their clearance by phagocytic cells. At a temperature of 25 °C, the zeta potential of the solution of PEGylated nanoshells used in our study was −25 mV for pH 5.6. The dynamic light scattering of gold nanoshells showed a good dispersion of gold nanoshells (supplementary Fig. S1A). The hydrodynamic size of PEGylated gold nanoshells in water was 185 nm (PDI 0.104). This was concordant with the result obtained in transmission electron microscopy (supplementary Fig. S1B). To determine the optimal dose of nanoshell to be injected in mice, we performed in vitro cytotoxicity test (MTT) using three types of cell lines, one normal human endothelial cell line (HUVEC) and two human cancer cell lines (CAKI 1, 786-0). We checked these cells lines for 24 h using different concentrations of gold nanoshells: 1.5×10^9 NP/mL, 3×10^9 NP/mL, 15×10^9 NP/mL, 3×10^{10} NP/mL. The concentration of 3×10^{10} NP/mL induced toxicity on the three cell lines, the concentration of 15×10^9 NP/mL induced toxicity on the tumor cell but not on the endothelial cell line. The concentration of 3×10^9 NP/mL was the highest concentration that did not induce any sign of toxicity on any of the three cell lines tested. This dose is in the range of doses previously tested by other teams, i.e between 10 μg/kg [16] and 8,000 μg/kg [17]. These previous studies focussed on early cytotoxic effect while we analysed in vivo both early and late toxic effects in our preclinical model. The late effect was assessed 6 months after injection because 6 months is a time point commonly used in clinics to assess chronic toxicity.

We analysed the uptake of these nanoshells from blood flow using ICP-MS because it is a sensitive method that enables detection of small quantities of gold [18]. As expected, we observed a decrease from Day 1 (381±111 ng/g) to Day 180 (1 ±1 ng/g), a time point when quantities of gold were nearly undetectable (Table 1). The uptake of gold spherical nanoparticles of 100, 200 and 250 nm, has been studied after intravenous injection in mice [19] and in rats [20]. The quantity of gold detected in blood by ICP-MS 24 h after injection was higher for 100-nm than for 250-nm gold nanoparticles in the experiments performed in rats [20] (Table 2), whereas no gold was detected in blood in the experiments performed in mice receiving 100-nm nanoparticles[19].

We systematically studied the biodistribution of PEGylated gold–silica nanoshells in organs of nude mice at different time points: Day 1, 15, 30, 60, 90 and 180. Using ICP-MS, we found a large amount of gold in the liver and spleen 24 h after injection (9,738±816 ng/g and 9,200±730 ng/g, respectively; Table 1). In the liver, the peak accumulation was observed at Day 30 (35,872±2,492 ng/g) with a significantly lower level when compared to Day 180 (3,723±376 ng/g) ($p<0.005$). In the spleen, we also found a large amount of gold at Day 1 (9, 200±730 ng/g). However, in the spleen the ICP-MS performed at different time points showed a progressive accumulation with a significant higher level when gold quantities at Day 1 (9,200±739 ng/g) were compared to gold quantities at Day 180 (33,857±2,564 ng/g) ($p<0.005$). Dark field analyses performed on liver and spleen tissue sections at 3 and 6 months after nanoparticle injections showed a large accumulation of gold nanoparticles in the two organs.

Table 1 Gold quantification in organs of normal non-xenografted nude mouse (ng/g of tissue) from Day 1 to Day 180

Tissues	Day 1	Day 15	Day 30	Day 60	Day 90	Day 180
Blood	381 (±111)	197 (±50)	147 (47)	99 (±28)	43 (±12)	1 (±1)
Liver	9,738 (±816)	16,615 (±800)	35,872 (±2,492)	16,601 (±765)	8,187 (±534)	3,723 (±376)
Bone marrow	13 (±8)	70 (±23)	57 (±13)	20 (±5)	19 (±9)	19 (±5)
Spleen	9,200 (±730)	13,511 (±2,360)	19,398 (±635)	21,406 (±1,956)	27,654 (±300)	33,857 (±2,564)
Kidney	395 (±19)	309 (±34)	161 (±45)	126 (±36)	29 (±15)	61 (±20)
Lung	55 (±21)	43 (±13)	54 (±12)	15 (±12)	21 (±12)	17 (±12)
Adrenal gland	306 (±12)	76 (±20)	53 (±15)	56 (19)	21 (±6)	47 (±6)
Lymph node	135 (±27)	239 (±73)	208 (±77)	255 (±75)	146 (±66)	120 (±25)
Ovary	46 (±14)	32 (±13)	12 (±6)	15 (±6)	10 (±8)	32 (±27)
Heart	14 (±5)	17 (±7)	13 (±5)	18 (±6)	15 (±7)	8 (±3)
Brain	12 (±4)	5 (±5)	1 (±1)	11 (±2)	5 (±3)	7 (±4)

Table 2 Comparative assessment of early and late toxic effects in our study and eight previously published studies

Nanoparticles		Administration			Protocol			Toxic effect	
Ref	Size (nm)	PEG	IV/IP	Dose	Injection number	Animal	Methods of analysis	Time of analysis	Early	Late (73 months)
Our study	130–150	Yes	IV	160 μg/kg	1	Mouse	ICP-MS, H&E, TEM	Min 5, 30; Day 1, 7, 15, Months 1, 2, 3, 6	No	No
[20]	10, 50, 100, 250	No	IV	80–120 μg/g	1	Rat	ICP-MS	Day 1	No	No
[3]	150	Yes	IV	2,550–3,775 μg/g	1, 3, 5	Mouse	NAA	Day 1, 3, 5	No	-
[6]	155	Yes	IV	2,340 μg/kg	1	Mouse	H&E, NAA	Day 1, 7, 28, 56, 182, 404	No	No
[9]	10, 50, 100, 200	No	IV	1,000 μg/kg	1	Mouse	ICP-MS	Day 1	No	-
[29]	40	No	IV	1,400–1,600 μg/kg	1	Mouse	ICP-MS, AMG stain	Day 1; Months 1, 3, 6	No	No
[17]	3, 5, 8, 12, 17, 37, 50	No	IP	8,000 μg/kg	1	Mouse	H&E	Day 21	Yes (liver, lung)	-
[30]	5, 25	No	IV	1,000 μg/kg	1	Rabbit	ICP-MS,TEM	Day 1	No	-
[16]	20	No	IV	10 μg/kg	1	Rat	ICP-MS	Days 1, 7; Months 1, 2	-	-
[18]	12, 5	No	IP	320, 1,600, 3,200 μg/kg	8	Mouse	ICP-MS, GF-AAS	Day 8	No	-

PEG poly-etylene glycol, *IV* intravenous, *IP* intraperitoneal, *min* minutes, *M* month, *ICP-MS* inductively coupled plasma-mass specrometry, *H&E* hematoxylin and eosin staining, *NAA* neutron activation analysis, *TEM* transmission eletron microscopy, *GF-AAS* graphite furnace atomic absorbtion, *IHC* immunohistochemistry

Comparison of the density of the nanoparticles at the two time points showed an increase in the spleen and a decrease in the liver, thus confirming the results obtained with ICP-MS (Fig. 1). The large accumulation of gold nanoparticles in the liver and spleen, also observed in mice for different size of spherical gold nanoparticles [20], could be linked to the fact that the capillaries in the spleen and liver are discontinuous [2] and lined by cells with phagocytic capacity. Phagocytic cells, particularly macrophages, are more numerous in the spleen than in the liver [21] and this fact could explain the discrepancy between the progressive diminution of gold nanoparticles in the liver and the progressive accumulation in the spleen. In addition, experimental data on mouse Kupffer cells, i.e. liver phagocytic cells, following intravenous injection of bacteriophage [22] demonstrated that after initial phagocytosis, there was an immediate and rapid decrease in the number of plaque-forming units (PFU) which could be recovered from both liver and spleen; however, as soon as 3 days after injection, the number of PFU which could be recovered from the spleen was greater than that found in the liver. At Day 5, there was as many as 50 times more PFU in the spleen than in the liver. In the present study, we assessed a concentration of gold nanoparticles ten times greater in the spleen than in the liver 6 months after injection.

We performed systematic pathological analyses to assess signs of toxicity at the different time points when the different organs of nude mice were analysed: Days 1, 15, 30, 60 and 180. We did not detect any signs of acute toxicity such as hypoplasia or complete aplasia of the bone marrow; acute nephrotoxicity with endothelial damage, fibrin deposit in the glomerular areas and necrosis of epithelial tubular cells; or cardiotoxicity with endocardial damage.

Regarding long-term toxicity, the greatest concentration of PEGylated gold silica nanoshells was found in the liver and spleen. Therefore, after dark field analysis, the same tissue sections from the liver and spleen 3 and 6 months after gold nanoshell injection were analysed using bright field microscopy to detect signs of toxicity. As shown in Fig. 1, no necrotic cell, no fibrosis and no inflammatory infiltrate were found. This is in accordance with the absence of any abnormalities in the clinical score used for the mouse follow-up. No similar study on long-term organ toxicity has been performed, as far as we know, in preclinical models.

In our study, we injected intravenously a single dose of 160 μg/kg gold nanoshells and we did not observe any toxicity either at early or long term. In three other studies using intravenous injection of gold nanoshells with a diameter larger than 100 nm, no toxicity was observed [13, 14], even in cases of repeated injections [3]. An early toxic effect on the liver and the lung was observed in only one mouse series, for gold particles of 8 to 37 nm of diameter injected intraperitoneally. As far as we know, only one previously published study focussed on long-term effect at 6 months [18]. It was different from our study by

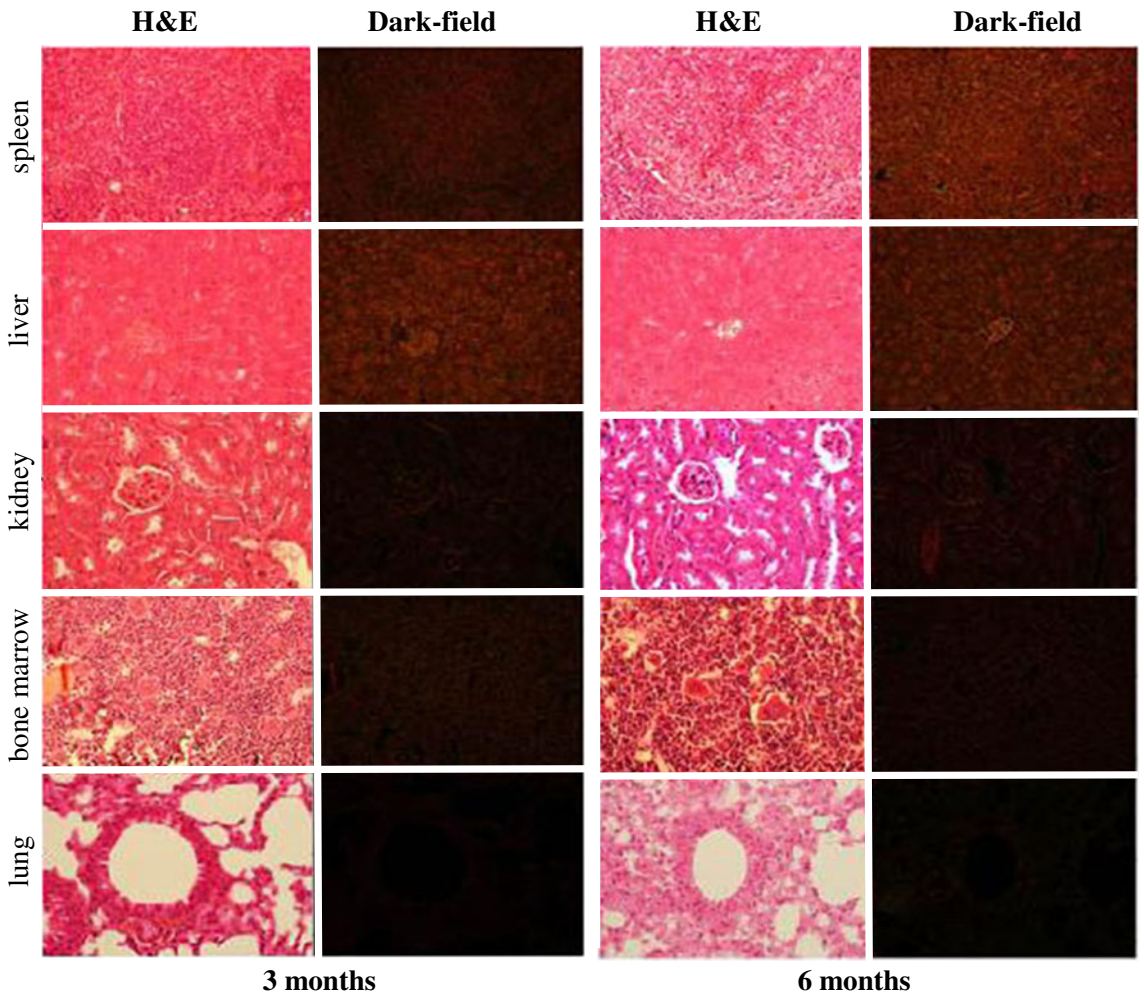

Fig. 1 Long-term toxicity study. Data obtained at late time points in normal non-xenografted nude mouse. Systematic histological analysis (H&E staining), 3 and 6 months after injection, in the spleen, liver, bone marrow and lung, did not show any tissue damage linked to toxicity, such as necrosis, fibrin deposit in vascular areas, inflammatory infiltrate, fibrosis or bone marrow hypoplasia or aplasia. Dark field microscopy analysis on the same areas, at the same time points, shows a high intensity signal in the liver and spleen at 3 months followed at 6 months by a decrease in the liver and an increase in the spleen. A very weak signal is detected in the kidney at 3 and 6 months and no signal is observed in the bone marrow and lung at the same time points. Magnification ×400

the dose injected (1,400 vs 160 μg/kg) and the size of the nanoparticles (40 nm vs 150 nm) but no long-term toxicity was found, as in our study.

Apart from the liver and spleen, in the other organs analysed at different time points in normal nude mice, results of ICP-MS are also confirmed by dark field analyses, but the quantities of gold were much smaller than in the liver and spleen. The kidney is the organ where we detected the less low quantity of gold, with a decrease between Day 1 (395±19 ng/g) and Day 180 (61±20 ng/g). These data show that gold nanoparticles moved to the kidney, as expected, since the kidney physiological function is filtering the entire blood flow through the fenestrated endothelium of glomerular capillaries [23]. However, the urinary excretion was low and this was probably linked to the 5.5-nm size of the capillary endothelium pores [18, 24], far smaller than the 150-nm diameter of the gold silica nanoshells we had injected.

Fig. 2 Uptake of gold particles. Data obtained at early time points in ▶ nude mouse xenografted with human renal cancer. **a** Induced coupled plasma-mass spectrometry (ICP-MS) for gold quantification (logarithmic representation) in the blood, liver, spleen, bone marrow, kidney and tumor at 5 and 30 min, 2 and 6 h and Day 1, 7 and 15. A significant decrease is observed in the blood, bone marrow and tumor when gold quantities are compared at 5 and 30 min, reflecting the rapid uptake of gold particles in highly vascularized areas, whereas an increase is observed in the liver and spleen when gold quantities are compared at 5 min and 15 days, reflecting the progressive uptake and stock of gold nanoparticles in these organs rich in phagocytic cells. **b** Distribution of gold nanoparticles in the xenografted human renal cancer at the same early time points. Dark field analysis shows a preferential distribution of gold nanoparticles in capillary wall areas at 2 h and in tumor cells at Day 1. Transmission electron microscopy shows an uptake of gold nanoparticles by endothelial cells at 6 h with a distribution in both endothelial and tumoral cells at Day 1, followed by an uptake and stock in phagocytic cell cytoplasm at Day 7. *$p < 0.05$

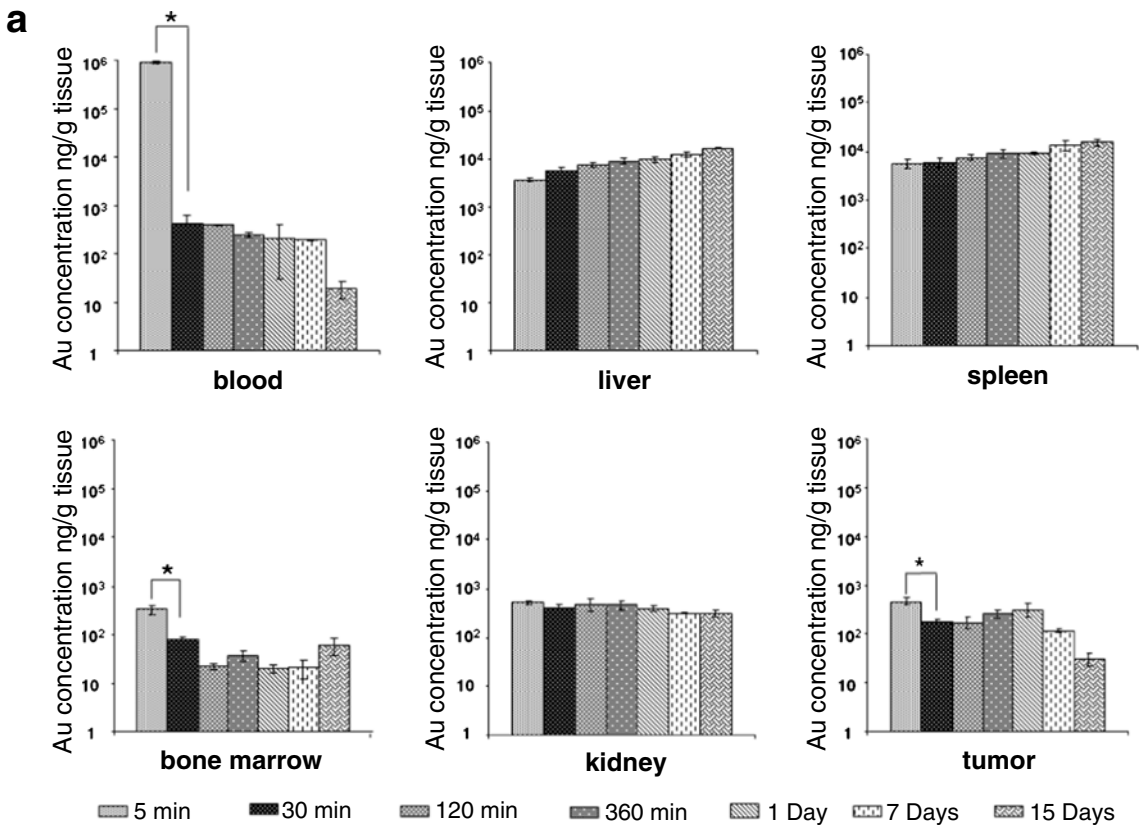
a
Au concentration ng/g tissue
blood
liver
spleen
bone marrow
kidney
tumor
5 min
30 min
120 min
360 min
1 Day
7 Days
15 Days

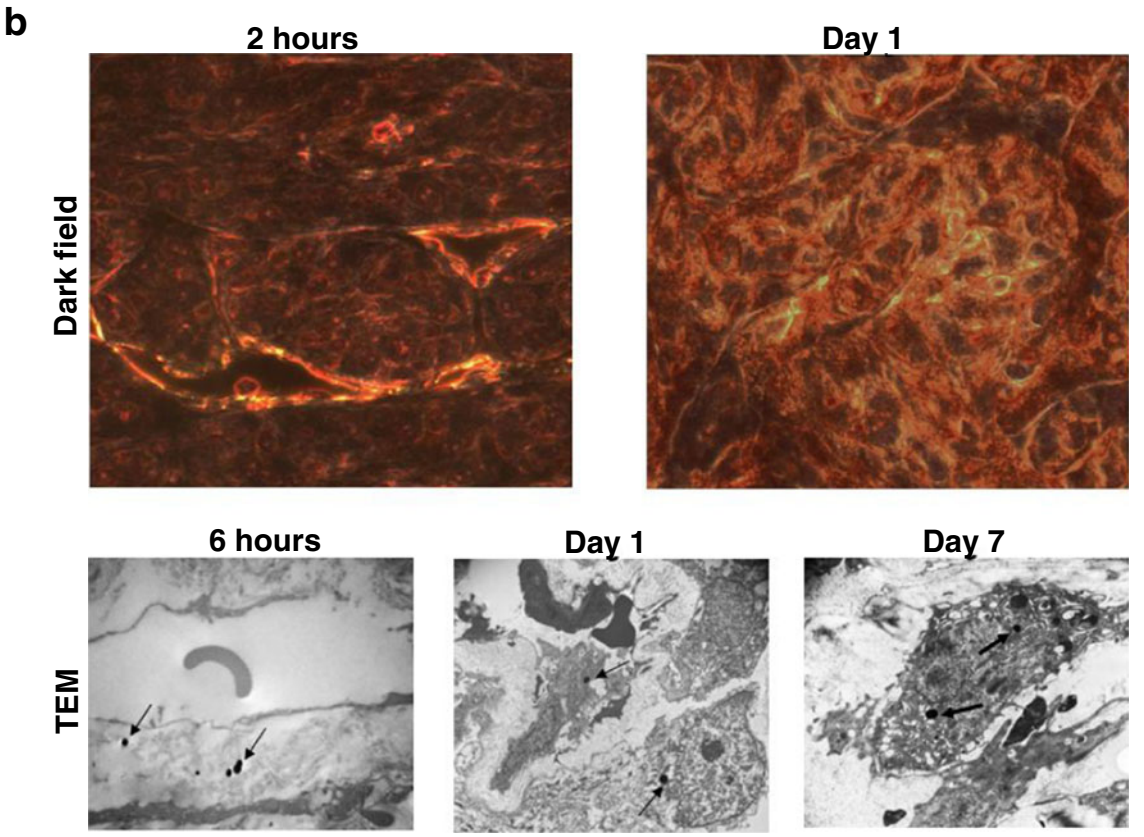
b
2 hours
Day 1
Dark field
6 hours
Day 1
Day 7
TEM

In the bone marrow (13±8 ng/g), lung (55±21 ng/g), adrenal gland (306±12 ng/g), lymph node (135±27 ng/g) and ovary (46 ±14 ng/g), very small gold quantities were detected at Day 1 and these quantities decreased over time (Table 1). In the brain, only traces of gold were found. This is in accordance with the clinical follow-up over 6 months since the mice did not show any behavioural abnormality, weight loss or mortality.

Regarding toxicity in the different organs studied, apart from the liver and spleen, pathological analyses of tissue sections of different time points did not show any signs of thrombosis, fibrin deposits or inflammatory infiltrate in the glomeruli at early time points and no glomerular sclerosis, interstitial fibrosis or inflammatory infiltrate in the kidney at late time points. There was no sign of hypoplasia or complete aplasia of the bone marrow. No interstitial fibrosis or inflammatory infiltrate was detected in the lung or heart, whether at early or late time points (Fig. 1). These data, provided by our preclinical model, are important because the treatment of cancer associating radiotherapy and poly-chemotherapy can induce vascular and interstitial damages in the kidney and heart [25], and life-threatening damages such as diffuse pulmonary fibrosis, and bone marrow aplasia. These severe complications linked to radiotherapy and poly-chemotherapy are systematically sought during follow-up of cancer patients under treatment and it is important to demonstrate that the uptake and the accumulation of large spherical gold silica nanoshells do not, on its own, induce any systemic organ damage.

This absence of toxicity, at early and late time points, on the organs most sensitive to efficient anticancer drugs enables further applications of gold nanoshells for local delivery of drugs on cells targeted through specific antibodies [26].

The study on xenografted mice was focussed on the tumor xenograft, but we also systematically studied the organs at different time points: 5 and 30 min, 2 and 6 h and 1, 7, 15 days (Fig. 2a).

When we compared the gold quantities detected by ICP-MS and gold nanoshell distribution in tissues using dark field analysis, we did not find any significant difference in the different organs of normal nude mice and of the xenografted nude mice. This implies that the engraftment of the human renal cancer did not change significantly the systemic distribution of large gold nanoshells after intravenous injection.

Regarding the xenografted human renal cancer, we successively studied the uptake of gold nanoshells from the blood and their distribution in the different cellular components of the tumor: tumor cells, microvessels, phagocytic interstitial cells.

When we compared the gold quantities in blood and xenograft at different time points, we found that in the two types of samples the larger amounts were found at the first time points (5 min), with a decrease at the successive time points, and significantly smaller gold quantities at Day 15 compared to the 5-min time point. These kinetic particularities were not found in the liver, spleen, bone marrow or kidney (Fig. 2a). These kinetic data in the blood and xenografted tumor could be linked to the fact that human renal cancer is a highly vascularised malignant tumor [11], and that the microvessels of malignant tumors are dystrophic with possible absence of pericytes, irregular thickness or absence of continuity of basement membrane [27]. In addition, experimental data in mice have demonstrated that gold nanoparticles are able to pass through large gaps in endothelial cells and accumulate into interstitial spaces [3]. This phenomenon is known as the enhanced permeability and retention effect (EPR effect) [28].

To precisely determine the distribution of large gold nanoshells in the different cellular components of the human renal cancer, we used two imaging methods: dark field and TEM.

Gold nanoshells could be detected in tumor sections using dark field microscopy as early as 5 min after injection. They remained located within the microvessels as long as 2 h (Fig. 2b). There was a striking distribution change between Day 1 and Day 15, with a distribution within cytoplasm of cells located outside the microvessel network. Transmission electron microscopy confirmed these results and enabled a more precise analysis at higher magnification. As early as 6 h after injection, gold nanoshells, easily detected because they are electron dense with a regular round shape and a constant diameter, were found in the sub-endothelial compartment, thus showing they had crossed over the microvessel endothelial wall. At Day 1, gold nanoshells could be detected both in the cytoplasm of microvessel endothelial cells and in the cytoplasm of tumor cells. After Day 7, gold nanoshells were mainly found within the cytoplasm of macrophages, easily identified because of their phagolysosomes. Rare nanoshells were detected into the cytoplasm of tumor cells at Day 15 (supplementary Fig. 2).

This original sequence not previously reported, using TEM to identify the different cell components of human renal cancer, opens new fields for medical applications using large PEGylated gold nanoshells by optimising the time for targeted hyperthermia or local drug delivery to tumor cells.

Acknowledgments We thank Tumorothèque Hopital Saint Louis; S Arien and K Pereira for the electron microscopy technique, N Sanson for the DLS and zeta potential measurements and A Swaine for the revision of the English language. Grants are from the ANR Golden Eye and Plan Cancer 2009-2013-projet GoldFever, ANR Ibisa.

Conflict of interest The authors declared no conflict of interest.

References

1. Wang Y, Black KC, Luehmann H, Li W, Zhang Y, Cai X, Wan D, Liu SY, Li M, Kim P, Li ZY, Wang LV, Liu Y, Xia Y (2013) Comparison study of gold nanohexapods, nanorods, and nanocages for photothermal cancer treatment. ACS Nano 7:2068–2077
2. Papasani MR, Wang G, Hill RA (2012) Gold nanoparticles: the importance of physiological principles to devise strategies for targeted drug delivery. Nanomedicine 8:804–814
3. Puvanakrishnan P, Park J, Diagaradjane P, Schwartz JA, Coleman CL, Gill-Sharp KL, Sang KL, Payne JD, Krishnan S, Tunnell JW (2009) Near-infrared narrow-band imaging of gold/silica nanoshells in tumors. J Biomed Opt 14:024044
4. Day ES, Thompson PA, Zhang L, Lewinski NA, Ahmed N, Drezek RA, Blaney SM, West JL (2011) Nanoshell-mediated photothermal therapy improves survival in a murine glioma model. J Neurooncol 104:55–63
5. Liu H, Liu T, Wang H, Li L, Tan L, Fu C, Nie G, Chen D, Tang F (2013) Impact of PEGylation on the biological effects and light heat conversion efficiency of gold nanoshells on silica nanorattles. Biomaterials 34:6967–6975
6. Gad SC, Sharp KL, Montgomery C, Payne JD, Goodrich GP (2012) Evaluation of the toxicity of intravenous delivery of auroshell particles (gold-silica nanoshells). Int J Toxicol 31:584–594
7. Chatelut E, Delord JP, Canal P (2003) Toxicity patterns of cytotoxic drugs. Invest New Drugs 21:141–148
8. Keefe DM, Bateman EH (2012) Tumor control versus adverse events with targeted anticancer therapies. Nat Rev Clin Oncol 9:98–109
9. Taurin S, Nehoff H, Greish K (2012) Anticancer nanomedicine and tumor vascular permeability; Where is the missing link? J Control Release 164(3):265–75
10. Varna M, Ratajczak P, Ferreira I, Leboeuf C, Bousquet G, Janin A (2012) In vivo distribution of inorganic nanoparticles in preclinical models. J Biomater Nanobiotechnol 3:269–279
11. Huang D, Ding Y, Li Y, Luo WM, Zhang ZF, Snider J, Vandenbeldt K, Qian CN, Teh BT (2010) Sunitinib acts primarily on tumor endothelium rather than tumor cells to inhibit the growth of renal cell carcinoma. Cancer Res 70:1053–1062
12. Varna M, Lehmann-Che J, Turpin E, Marangoni E, El-Bouchtaoui M, Jeanne M, Grigoriu C, Ratajczak P, Leboeuf C, Plassa LF, Ferreira I, Poupon MF, Janin A, de The H, Bertheau P (2009) p53 dependent cell-cycle arrest triggered by chemotherapy in xenografted breast tumors. Int J Cancer 124:991–997
13. Bardhan R, Lal S, Joshi A, Halas NJ (2011) Theranostic nanoshells: from probe design to imaging and treatment of cancer. Acc Chem Res 44:936–946
14. Thakor AS, Jokerst J, Zavaleta C, Massoud TF, Gambhir SS (2011) Gold nanoparticles: a revival in precious metal administration to patients. Nano Lett 11:4029–4036
15. Kah JC, Wong KY, Neoh KG, Song JH, Fu JW, Mhaisalkar S, Olivo M, Sheppard CJ (2009) Critical parameters in the pegylation of gold nanoshells for biomedical applications: an in vitro macrophage study. J Drug Target 17:181–193
16. Balasubramanian SK, Jittiwat J, Manikandan J, Ong CN, Yu LE, Ong WY (2010) Biodistribution of gold nanoparticles and gene expression changes in the liver and spleen after intravenous administration in rats. Biomaterials 31:2034–2042
17. Chen YS, Hung YC, Liau I, Huang GS (2009) Assessment of the in vivo toxicity of gold nanoparticles. Nanoscale Res Lett 4:858–864
18. Lasagna-Reeves C, Gonzalez-Romero D, Barria MA, Olmedo I, Clos A, Sadagopa Ramanujam VM, Urayama A, Vergara L, Kogan MJ, Soto C (2010) Bioaccumulation and toxicity of gold nanoparticles after repeated administration in mice. Biochem Biophys Res Commun 393:649–655
19. Sonavane G, Tomoda K, Makino K (2008) Biodistribution of colloidal gold nanoparticles after intravenous administration: effect of particle size. Colloids Surf B: Biointerfaces 66:274–280
20. De Jong WH, Hagens WI, Krystek P, Burger MC, Sips AJ, Geertsma RE (2008) Particle size-dependent organ distribution of gold nanoparticles after intravenous administration. Biomaterials 29: 1912–1919
21. Nagayama S, Ogawara K, Fukuoka Y, Higaki K, Kimura T (2007) Time-dependent changes in opsonin amount associated on nanoparticles alter their hepatic uptake characteristics. Int J Pharm 342:215–221
22. Inchley CJ (1969) The actvity of mouse Kupffer cells following intravenous injection of T4 bacteriophage. Clin Exp Immunol 5: 173–187
23. Molema G, Aird WC (2012) Vascular heterogeneity in the kidney. Semin Nephrol 32:145–155
24. Alkilany AM, Murphy CJ (2010) Toxicity and cellular uptake of gold nanoparticles: what we have learned so far? J Nanopart Res 12:2313–2333
25. Khouri MG, Douglas PS, Mackey JR, Martin M, Scott JM, Scherrer-Crosbie M, Jones LW (2012) Cancer therapy-induced cardiac toxicity in early breast cancer: addressing the unresolved issues. Circulation 126:2749–2763
26. You J, Zhang R, Xiong C, Zhong M, Melancon M, Gupta S, Nick AM, Sood AK, Li C (2012) Effective photothermal chemotherapy using doxorubicin-loaded gold nanospheres that target EphB4 receptors in tumors. Cancer Res 72:4777–4786
27. Dvorak HF, Weaver VM, Tlsty TD, Bergers G (2011) Tumor microenvironment and progression. J Surg Oncol 103:468–474
28. Maeda H, Wu J, Sawa T, Matsumura Y, Hori K (2000) Tumor vascular permeability and the EPR effect in macromolecular therapeutics: a review. J Control Release 65:271–284
29. Sadauskas E, Danscher G, Stoltenberg M, Vogel U, Larsen A, Wallin H (2009) Protracted elimination of gold nanoparticles from mouse liver. Nanomedicine 5:162–169
30. Glazer ES, Zhu C, Hamir AN, Borne A, Thompson CS, Curley SA (2011) Biodistribution and acute toxicity of naked gold nanoparticles in a rabbit hepatic tumor model. Nanotoxicology 5:459–468